Nearly Singular Magnetic Fluctuations in the Normal State of a High-T_c Superconductor

G. Aeppli[1,2], T. E. Mason[2,3], S. M. Hayden[4], H. A. Mook[5], and J. Kulda[6]
[1] *NEC Research Institute, 4 Independence Way, Princeton, NJ 08540, USA*
[2] *Risø National Laboratory, 4000 Roskilde, Denmark*
[3] *Dept. of Physics, University of Toronto, Toronto, Canada M5S 1A7*
[4] *Dept. of Physics, University of Bristol, Bristol BS8 1TL, United Kingdom*
[5] *Oak Ridge National Laboratory, Oak Ridge, TN 37831, U.S.A.*
[6] *Institut Laue-Langevin, BP 156X, Grenoble Cedex, France*
(Science, **278**, 21 November 1997, p. 1432-1435)

Polarized and unpolarized neutron scattering was used to measure the wave vector- and frequency-dependent magnetic fluctuations in the normal state (from the superconducting transition temperature, $T_c = 35$, up to 350 K) of single crystals of $La_{1.86}Sr_{0.14}CuO_4$. The peaks which dominate the fluctuations have amplitudes that decrease as T^{-2} and widths that increase in proportion to the thermal energy, $k_B T$ (where k_B is Boltzmann's constant), and energy transfer added in quadrature. The nearly singular fluctuations are consistent with a nearby quantum critical point.

The normal state of the metallic cuprates is as unusual as their superconductivity. For example, the electrical resistivity of samples with optimal superconducting properties is linear in temperature (T) from above 1000 K to T_c [1]. Correspondingly, infrared reflectivity reveals charge fluctuations with a characteristic energy scale that is proportional only to T [1,2]. Furthermore, the effective number of charge carriers, as measured with the classic Hall effect, is strangely T-dependent. Even so, the Hall angle, a measure of the deflection of carriers in the material by an external magnetic field, follows a T^{-2} law [3]. Thus, the metallic charge carriers in the doped cuprates exhibit peculiar but actually quite simple properties [4] in the normal state. Also, these properties do not vary much between the different high-T_c families.

Electrons carry spin as well as charge, so it is reasonable to ask whether the normal state magnetic properties, derived from the spins, are as simple and universal as those derived from the charges. Experiments to probe the spins include classical magnetic susceptometry, where the magnetization in response to a homogeneous external magnetic field is measured, and resonance experiments, where nuclear dipole and quadrupolar relaxation is used to monitor the electron spins. The spin-sensitive measurements yield more complex and less universal results than those sensitive to charge, and indeed do not seem obviously related to the frequency-dependent conductivity, $\sigma(\omega, T)$, probed in electrical, microwave and optical experiments. In particular, there is little evidence for magnetic behavior which is as nearly singular, in the sense of diverging (for $T \to 0$) amplitudes, time constants, or length scales, as the behavior of $\sigma(\omega, T)$.

We report nearly singular behavior of the magnetic fluctuations in the simplest of high-T_c materials, namely, the compound $La_{2-x}Sr_xCuO_4$ whose fundamental building blocks are single CuO_2 layers, as determined by inelastic magnetic neutron scattering. A beam of mono-energetic neutrons is first prepared and then scattered from the sample, and the outgoing neutrons are labeled according to their energies and directions to establish an angle and energy-dependent scattering probability, or cross-section, $d^2\sigma/d\omega d\Omega$. Because the neutron spin and the electron spins in the sample interact through magnetic dipole coupling, the cross-section is directly proportional to the magnetic structure function, $S(\mathbf{Q}, \omega)$, the Fourier transform of the space- and time-dependent two-spin correlation function. The momentum and energy transfers $\mathbf{Q}$ and ω are simply the differences between the momenta and energies of the ingoing and outgoing neutrons, respectively. Via the fluctuation-dissipation theorem, $S(\mathbf{Q}, \omega)$ is in turn proportional to the imaginary part, $\chi''(\mathbf{Q}, \omega)$, of the generalized linear magnetic response $\chi(\mathbf{Q}, \omega)$. The bulk susceptibility measured using a magnetometer is the long-wavelength, small-wavenumber, ($\mathbf{Q} \to 0$), limit of $\chi'(\mathbf{Q}, \omega = 0)$, while the nuclear resonance techniques are averages of $\chi''(\mathbf{Q}, \omega \sim 0)$ over momenta $\mathbf{Q}$ which are of order inverse interatomic spacings.

Figure 1 **A** is a schematic phase diagram for $La_{2-x}Sr_xCuO_4$ as a function of T, hole doping (x), and pressure (y). Holes and pressure are generally introduced chemically, most notably through substitution of Sr^{2+} and Nd^{3+} ions, respectively, for the La^{3+} ions in La_2CuO_4 [5,6]. Possible magnetic ground states range from simple antiferromagnetic (AF for $x \sim 0$) to a long-period spin density wave with strong coupling to the underlying lattice (shown as a gray "mountain" for $x \sim 0.1$ in Fig. 1 **A**). Unit cell doubling, where the spin on each Cu^{2+} ion is antiparallel to those on its nearest neighbors displaced by vectors $(0, \pm a_o)$ and $(\pm a_o, 0)$ in the (nearly) square CuO_2 planes, characterizes

the simple AF state [7]; the lattice constant, $a_o = 3.8$ Å . The associated magnetic Bragg peaks, observed by neutron scattering, occur at reciprocal lattice vectors $\mathbf{Q}$ of the form $(n\pi, m\pi)$, where n and m are both odd integers; the axes of the reciprocal lattice coordinate system are parallel to those of the underlying square lattice in real space. Substitution of Sr for La introduces holes into the CuO_2 planes, and initially replaces the AF phase by a magnetic (spin) glass phase. It is for this non-superconducting composition regime, where the magnetic signals are strong and for which large single crystals have long been available, that the most detailed T-dependent magnetic neutron scattering studies have been performed [8]. With further increases in Sr content, the magnetic glass phase disappears and superconductivity emerges. At the same time, the commensurate peak derived from the order and fluctuations in the non-superconducting sample splits into four incommensurate peaks, as indicated in Fig. 1 **B** [9]. These peaks are characterized by a position, an amplitude, and a width. Previous work [9] describes how the peak positions vary with composition at low temperatures. The new contribution of the present report is to follow the red trajectory in Fig. 1 and so obtain the T and ω dependence of the amplitude and width, which represent the maximum magnetic response and inverse magnetic coherence length, respectively.

The $La_{1.86}Sr_{0.14}CuO_4$ crystals used here are the same as those used in our previous determination [10] of $\chi''(\mathbf{Q}, \omega)$ around and below the superconducting transition at $T_c = 35$ K. Unpolarized measurements, where the spins of the in-going and outgoing neutrons are unspecified, were carried out using the TAS6 spectrometer of the Risø DR3 reactor in the same configuration employed before [10]. We performed measurements with fully polarized in-going and outgoing beams using the IN20 instrument at the Institut Laue-Langevin in Grenoble, France.

Our surveys of $\mathbf{Q} - \omega$ space at various Ts is summarized in Fig. 2. Frame **A** shows scans along the solid red line in Fig. 1 **B** through the incommensurate peaks at $[\pi(1-\delta), \pi]$ and $[\pi, \pi(1+\delta)]$ for energy transfer $\hbar\omega$ fixed at 6.1 meV (Fig. 2 **A**). We have checked that the peaks are of purely magnetic origin by using polarized neutrons (Fig. 2 **B**). The spin-flip (SF) channel contains background plus magnetic scattering whereas the non spin-flip (NSF) channel contains background plus phonon scattering. The incommensurate response only occurs in the SF channel, confirming that it is derived from the electron spins.

The most important result in Fig. 2 **A** is that the sharp peaks at 80 K broaden to nearly merge at 297 K, an effect also illustrated in Fig. 2 **C** and **D**, which illustrate the Q- and $\omega-$ dependence of $\chi''(\mathbf{Q}, \omega)$ determined by using the fluctuation dissipation theorem, $\chi''(\mathbf{Q}, \omega)\ (n(\omega) + 1) = S(\mathbf{Q}, \omega)$, where $n(\omega) + 1 = 1/(1 - e^{-\hbar\omega/k_B T})$ ($\hbar$ is Planck's constant divided by 2π and k_B is Boltzmann's constant). The magnetic structure function $S(\mathbf{Q}, \omega)$ is simply the scattering near the incommensurate peaks measured along the solid red line in Fig. 1 **B** and indicated by the filled symbols in **A**, minus the background indicated by the open symbols. Comparison of Fig. 2 **C** and 2 **D** shows that warming from T_c (35 K) to 297 K gives a much smaller $\chi''(\mathbf{Q}, \omega)$, and eliminates clear incommensurate peaks at all energies $\hbar\omega$ probed. At intermediate Ts there is more modest broadening of the magnetic peaks at low $\hbar\omega$, as well as an intensity reduction which is much more pronounced at low than at high $\hbar\omega$.

Figure 3 **A** summarizes the dramatic evolution of the incommensurate peak amplitudes with $T > T_c$. Both unpolarized and polarized beam data are shown, and their consistency confirms the background subtraction procedure used in the faster unpolarized beam measurements. In addition, full polarization analysis [11] of the intensity at the position indicated by a blue dot in Fig. 1 **B** confirms that the increase with T seen in the background shown in Fig. 2 A is of non-magnetic origin.

We have so far given a qualitative survey of our data, which are astonishing because they display much greater temperature-sensitivity above the superconducting transition than any other magnetic neutron scattering data collected so far for a cuprate with composition nearly optimal for superconductivity. To describe more precisely the singular behaviors of the amplitude and widths of the incommensurate peaks, we must take into account the finite resolution of our instrument. We have consequently parametrized our data at each $\hbar\omega$ and T in terms of the convolution of the instrumental resolution and the general form [12],

$$S(\mathbf{Q}, \omega) = \frac{[\mathrm{n}(\omega) + 1]\chi''_{\mathrm{P}}(\omega, \mathrm{T})\kappa^4(\omega, \mathrm{T})}{[\kappa^2(\omega, \mathrm{T}) + \mathrm{R}(\mathbf{Q})]^2} \ . \tag{1}$$

$\mathrm{R}(\mathbf{Q})$ is a function, with the full symmetry of the reciprocal lattice and dimensions of $|\mathbf{Q}|^2$, which is everywhere positive except at zeroes coinciding with the incommensurate peak positions. From this definition, it follows that $\chi''_{\mathrm{P}}(\omega, \mathrm{T})$ (in absolute units via a standard phonon-based calibration [13]) is the peak susceptibility and $\kappa(\omega, \mathrm{T})$ is an inverse length scale measuring the sharpness of the peaks. To perform fits, we have expanded $\mathrm{R}(\mathbf{Q})$ near (π, π) to lowest order in q_x and q_y, the components of $\mathbf{Q}$ relative to (π, π),

$$\mathrm{R}(\mathbf{Q}) = \frac{[(q_x - q_y)^2 - (\pi\delta)^2]^2 + [(q_x + q_y)^2 - (\pi\delta)^2]^2}{2(2\mathrm{a}_0\pi\delta)^2} \ . \tag{2}$$

Because all of our data show features at the incommensurate positions at which the low-T and $-\omega$ data are peaked, we simply fix δ at its low-T and $-\omega$ value of 0.245. The solid lines in Fig. 1 **A** and **B** correspond to Eq. 1 convolved with the instrumental resolution with parameters $\kappa(\omega, T)$ and $\chi''_{\mathrm{P}}(\omega, T)$ chosen to obtain the best fit; that the data and fits are indistinguishable attests to the adequacy of Eq. 1 as a description of our measurements.

We discuss first the peak amplitudes $\chi''_{\mathrm{P}}(\omega, \mathrm{T})$, shown for three temperatures as a function of ω in Fig. 2 **E**. In agreement our earlier work [9], when these amplitudes are assembled to produce spectra as a function of ω for fixed Ts, there is no statistically significant evidence for a spin gap or even a pseudogap at any $\mathrm{T} \geq T_c$. Furthermore, only for the lowest T (35 K), is there an identifiable energy scale below 15 meV. For 35K, the scale is the ~ 7 meV energy transfer beyond which the peak spectrum flattens out. Otherwise, all of the data are in the low-ω regime where $\chi''_{\mathrm{P}}(\omega, \mathrm{T})$ is proportional to ω. This means that at each $\mathrm{T} \geq 85$ K our measurements are characterized by a single amplitude parameter, namely $\chi''_{\mathrm{P}}(\omega, \mathrm{T})/\omega$. Even for 35 K $\leq T \leq$ 85 K, this is true for $\hbar\omega < 5$ meV. We consequently shift our attention to the detailed T-dependence, shown in Fig. 3 **B**, of the low-frequency limit of $\chi''_{\mathrm{P}}(\omega, T)/\omega$.

The remarkable result is that the peak amplitude, after correction for resolution broadening effects, changes by two orders of magnitude over the one order of magnitude rise in temperature from $T_c = 35$ K. Indeed, a $\mathrm{T}^{-\alpha}$ law with $\alpha = 1.94 \pm 0.06 \cong 2$ describes the decrease of $\chi''_{\mathrm{P}}(\omega, \mathrm{T})/\omega$ with increasing T, indicating a divergence in the $T \to 0$ limit that is interrupted by the superconducting transition.

We turn now to how the inverse length $\kappa(\omega, \mathrm{T})$ depends on T and ω. The behavior, shown in Fig. 3 **C** appears complicated, apart from the fact that raising either T or ω increases $\kappa(\omega, \mathrm{T})$. However, closer inspection reveals that similar increases are associated with frequencies ω and temperatures T where $\mathrm{k_B T} \approx \hbar\omega$. Fig. 4, which shows $\kappa(\omega, \mathrm{T})$ plotted against $\sqrt{\mathrm{T}^2 + (\hbar\omega/\mathrm{k_B})^2}$, makes the interchangeablitity of temperature and frequency obvious. Here, the $\kappa(\omega, \mathrm{T})$ values for different ω's cluster near a single line with inverse slope 2000 $(\text{Å}\mathrm{K})^{-1} \cong \frac{1}{3}\mathrm{Ja_0/k_B}$, where J is the exchange constant of pure La_2CuO_4 [14] Correspondingly, the solid curve in the figure for which:

$$\kappa^2 = \kappa_o^2 + a_o^{-2}[(\mathrm{k_B T/E_T})^2 + (\hbar\omega/\mathrm{E}_\omega)^2]^{1/Z} \;, \tag{3}$$

$Z = 1$, $\kappa_0 = 0.034$ Å^{-1}, and $\mathrm{E_T} = \mathrm{E}_\omega = 47\mathrm{meV} \cong \frac{1}{3}\mathrm{J}$, gives a good description of the data.

As a classical spin system approaches a magnetic phase transition, the magnetic susceptibility and correlation length typically diverge. We have discovered that the normal state magnetic response of $La_{1.86}Sr_{0.14}CuO_4$ is characterized by nearly diverging amplitude and length scales. Thus, we are near to a low-T or zero-T phase transition. The latter is commonly referred to as a quantum critical point(QCP) [15,16], which occurs at T=0 and $\hbar\omega = 0$ in a phase space labeled by T, $\hbar\omega$, and a quantum fluctuation parameter α. The lower inset of Fig. 4 shows such a phase space where the solid circle marks the QCP. As for ordinary critical points, the parameter defining the state of the system anywhere in the three-dimensional (3D) phase space is the inverse coherence length κ. For a fixed composition, such as our $La_{1.86}Sr_{0.14}CuO_4$ sample, α is fixed and experiments are performed in the $T - \hbar\omega$ plane drawn. Furthermore, α is associated with a particular inverse length κ_o when T and $\omega \to 0$. If we add to the graphic description of the inset in Fig. 4 the assumption of a Euclidean metric for measuring distances to the QCP, we immediately recover Eq. 3 with the dynamical critical exponent, Z=1. It turns out that theory for 2D quantum magnets supports the concept of the Euclidean metric and hence that Z=1. In addition, it posits that T and $\hbar\omega$ should be interchangeable, an idea labeled 'ω/T scaling' [4,8]. We have checked the extent to which our data support these ideas by allowing κ_o, Z, $\mathrm{E_T}$, and E_ω all to vary to yield the best fit of $\kappa(\omega, T)$. The outcome, namely that $\kappa_o = 0.033 \pm 0.004$ Å^{-1}, $\mathrm{E_T/k_B} = 590 \pm 100K$, $\mathrm{E}_\omega/\mathrm{k_B} = 550 \pm 120K$ and $\mathrm{Z} = 1.0 \pm 0.2$, supports a simple QCP hypothesis.

Beyond providing a framework for understanding ω- and T-dependent length scales, the QCP hypothesis also has consequences for the susceptibility amplitudes. Specifically, as $\omega \to 0$, $\chi''_{\mathrm{P}}(\omega, \mathrm{T})/\omega$ should be controlled by a single variable representing the underlying magnetic length. In the upper right corner of Fig. 4, we plot $\chi''_{\mathrm{P}}/\omega$ as a function of such a variable, namely $\kappa(\omega = 0, T)$. The outcome is that $\chi''_{\mathrm{P}}(\omega, \mathrm{T})/\omega$ is proportional to $\kappa(\omega = 0, T)^\delta$ where $\delta = (2 - \eta + Z)/Z = 3 \pm 0.3$, in agreement with theoretical expectations [16] for QCP's occurring in 2D insulating magnets.

To make the QCP hypothesis plausible, it would be useful to have evidence for an ordered state nearby in phase space. Because the high-T_c superconductors can be chemically tuned, what we are looking for are related compounds with magnetically ordered ground states. The most obvious is pure La_2CuO_4. However, beyond the material itself seeming far away in the phase space of Fig. 1 **A**, the simple unit cell doubling describing the antiferromagnetism of the material is remote from the long-period spin modulation which one would associate with the quartet of peaks seen in the magnetic response of $La_{1.86}Sr_{0.14}CuO_4$. More interesting compounds are found when the phase space is expanded to consider ternary compounds, where elements other or in addition to Sr are substituted onto the La site. When Nd is substituted for La while keeping the Sr site occupancy(x) and hence hole density at 1/8, the material is no longer superconducting but exhibits instead a low-temperature phase characterized by magnetic Bragg peaks - corresponding

to static magnetic order- at loci close to where the magnetic fluctuations are peaked in $La_{1.86}Sr_{0.14}CuO_4$. While the full ternary phase diagram has not been searched, we have sketched what it might look like in Fig. 1, where the grey phase emerging close to the superconducting state is the ordered 'striped phase' - so named because one model describes it in terms of stripes of antiferromagnetic material separated by lines of charges [17]. More generally, experiments on the high-T_c materials can be thought of as travels through a 3D phase space such as that depicted in Fig. 1 **A**, and the changes in behavior found on such travels can be associated with different features of the landscape coming into prominence depending upon the height from which they are observed. At the higher $\hbar\omega$'s and Ts, the (red) AF phase, characterized by a very high coupling constant($\sim$ 0.15 eV) is the most obvious feature. At the intermediate Ts we probed, the dominant feature is the gray mountain where 'striped' order has been found. Finally, at the lowest T, the superconducting instability dominates. The knowledge that the cuprates inhabit an interesting 3D phase space together with our discovery that the spin fluctuations in one high-T_c material are as singular as the charge fluctuations should simplify the task of understanding both the anomalous normal state properties and the high-Tc superconductivity of the cuprates.

---

[1] B. Batlogg et al., p.5 in *Electronic Properties of High-T_c Superconductors* (Springer, Berlin 1993).
[2] F. Slakey et al., Phys. Rev. B. **43**, 3764 (1991); Z. Schlesinger et al., Phys. Rev. Lett. **65**, 801 (1990).
[3] T.R. Chien et al., Phys. Rev. Lett. **67**, 2088 (1991).
[4] C.M. Varma et al., Phys. Rev. Lett. **63**, 1996 (1989).
[5] B. Büchner et al., Phys. Rev. Lett. **73**, 1841 (1994).
[6] J.M. Tranquada et al., Phys. Rev. Lett. **78**, 338 (1997) and Nature(London) **375**, 561 (1995).
[7] D. Vaknin et al., Phys. Rev. Lett. **58**, 2802 (1987).
[8] S.M. Hayden et al., Phys. Rev. Lett. **66**, 821 (1991); B. Keimer et al., Ibid **67**, 1930 (1991); B. Sternlieb et al., Phys. Rev. B**47**, 5320 (1993); J. Rossat-Mignod et al., Physica B **169**, 58 (1991).
[9] S.-W. Cheong et al., Phys. Rev. Lett **67**, 1791 (1991); T.E. Mason et al., Ibid **68**, 1414 (1992); T.R. Thurston et al., Phys. Rev. B **46**, 9128 (1992); M. Matsuda et al., Ibid **49**, 6958 (1994); K. Yamada et al.,preprint(1997).
[10] T.E. Mason et al., Phys. Rev. Lett. **71**, 919 (1993).
[11] R.M. Moon et al., Phys. Rev. **181**, 883 (1969).
[12] H. Sato and K. Maki, Int. J. Magn. **6**, 183 (1974); D.R. Noakes et al., Phys. Rev. Lett. **65**, 369 (1990).
[13] We have used acoustic phonons in scans along Q = $(2, \xi, 0)$ and (2,0, ν) (orthorhombic notation) for $\hbar\omega = 2$ and 2.7 meV (sound velocity $\cong$ 23meV$-$ Å).
[14] See e.g. S.M. Hayden et al., Phys. Rev. Lett. **67**, 3622 (1991) and D.C. Johnston, J. Magn. Magn. Mat. **100**, 218 (1991).
[15] See overview by M. Continentino, Physics Reports **39**, 179 (1994) and experiments by M.C. Aronson et al., Phys. Rev. Lett. **75**, 725 (1995), H.v. Löhneysen et al., Phys. Rev. Lett. **72**, 3262 (1994), and D. Bitko et al., Phys. Rev. Lett. **77**, 940 (1996), A. Husmann et al., Science **274**, 1874 (1996). Earlier theoretical papers include M. Rasolt et al., Phys. Rev. Lett. 53, 798 (1984) and S. Chakravarty et al. , Phys. Rev. B **39**, 2344 (1989).
[16] S. Sachdev and J. Ye, Phys. Rev. Lett. **69**, 2411 (1992); A. Chubukov et al., Phys. Rev. B **49**, 11919 (1994); A.J. Millis, Phys. Rev. B **48**, 7183 (1993).
[17] V.J. Emery and S.A. Kivelson, Physica **209**, 597 (1993); J. Zaanen and O. Gunnarsson, Phys. Rev. B **40**, 7391 (1989).

We thank B. Batlogg, S. Chakravarty, P. Littlewood, A. Millis, D. Pines, B. Statt, R. Walstedt, and especially S. Sachdev for many helpful conversations, K.N. Clausen, K. Bechgaard, and J. Kjems for hospitality at Risø, and ECLIP, EPSRC, NATO, NSERC, CIAR, and USDOE for support.

FIG. 1. **A** Schematic phase diagram for $La_{2-x}Sr_xCuO_4$ showing the evolution from long range antiferromagnetic (AF) order (x=0, T_N shown in red), through an intermediate spin glass (SG) phase (green) to superconducting (SC) order (blue). Double doping (with Nd on the La site for example) results in stripe phase ordering (gray) shown along the y axis. **B** Map of the region of reciprocal space (**Q** vector) near (π, π) probed in the current measurements. Typically data were taken along the red line over two of the four incommensurate peaks that occur in our x=0.14 sample with the background determined along the dashed green trajectory.

FIG. 2. **A** Scans collected with unpolarized neutrons at constant energy ($\hbar\omega = 6.1$ meV) along the trajectory shown as a red line in Fig. 1 **B** (parametrized by ξ where $\mathbf{Q} = \xi(\pi,\pi) + (\delta/2)(-\pi,\pi)$) through two incommensurate peak positions. Actual counting times were in the 10 to 60 minute per point range. Open symbols represent background collected along the trajectory indicated by the dashed green line in Fig. 1 **B**. Solid lines correspond to resolution-corrected structure factor defined by Eq. 1. **B** Polarized scans at constant energy ($\hbar\omega = 3.5$ meV) at 40 K showing the spin-flip and non spin-flip intensity. The incommensurate peaks occur only in the spin-flip channel confirming their magnetic origin. **C** and **D** Energy and momentum (along solid trajectory in Fig. 1 **B**) -dependent magnetic response function $\chi''(\mathrm{Q},\omega)$, derived from background corrected intensities using fluctuation-dissipation theorem at **C** 35 and **D** 297 K. No attempt has been made to correct for experimental resolution, which broadens and weakens sharp features in $\chi''(\mathrm{Q},\omega)$. Color scale corresponds to the raw background corrected intensities, measured per unit signal in the incident beam monitor, while the (vertical) numerical scales are in units of counts per six minutes divided by $[\mathrm{n}(\omega) + 1]$. **E** Resolution-corrected (incommensurate) peak values of the magnetic response as a function of frequency.

FIG. 3. Temperature dependence of **A** peak intensity derived from full polarization analysis [11] and unpolarized neutron data at 3.5 meV and **B** Resolution-corrected peak response divided by frequency in the low-frequency limit obtained from the fits described in the text. Absolute scale in **B** is from normalization to phonons [13]. **C** inverse length scale $\kappa(\omega, T)$ at various fixed energy transfers $\hbar\omega$.

FIG. 4. Temperature dependence of inverse length scale $\kappa(\omega,\mathrm{T})$ at various fixed energy transfers $\hbar\omega$ plotted against T and $\hbar\omega$ added in quadrature. The solid line corresponds to a Z = 1 quantum critical point (see Eq. 3 and text). The graph in the upper right shows how the peak response depends on $\kappa = \kappa(\omega = 0, T)$. The inset shows the three-dimensional space defined by ω,T, and a composition dependent control parameter α. The dark plane corresponds to the (ω,T) phase space probed by our x=0.14 sample while the solid circle represents a nearby quantum critical point.

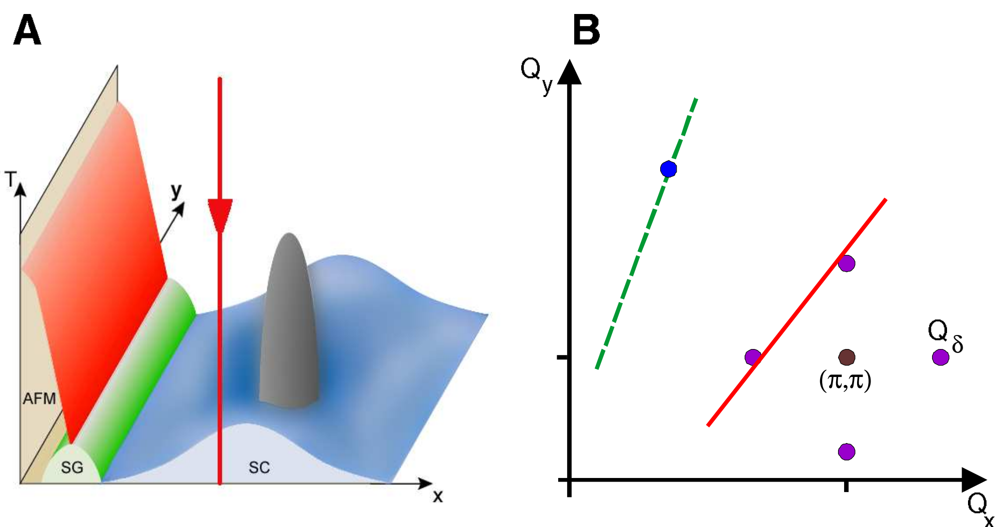
A
T
y
AFM
SG
SC
x
B
Q_y
Q_δ
(π,π)
Q_x

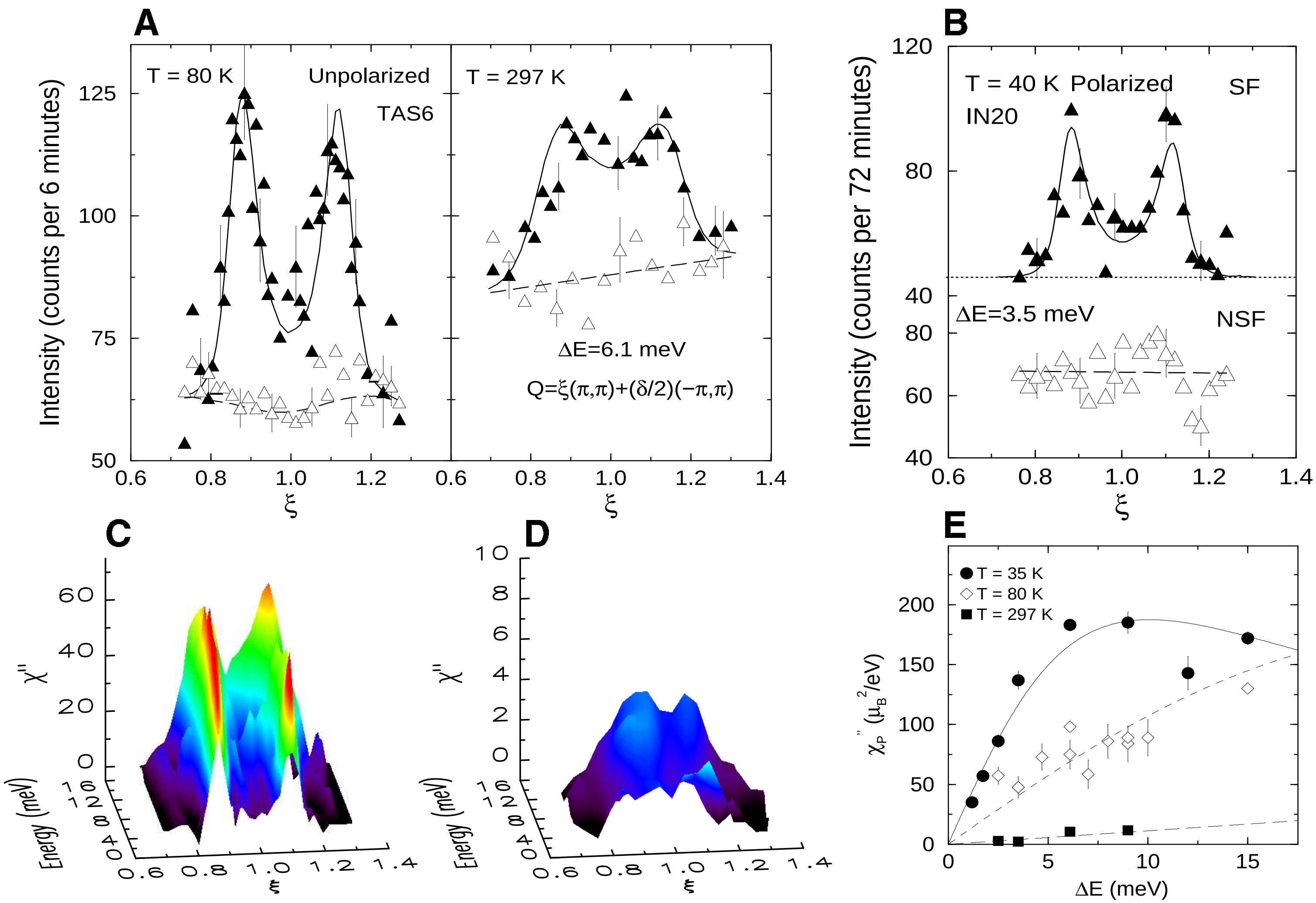
A
T = 80 K
Unpolarized
TAS6
T = 297 K
ΔE=6.1 meV
Q=ξ(π,π)+(δ/2)(−π,π)
Intensity (counts per 6 minutes)
ξ
B
T = 40 K Polarized
IN20
SF
NSF
ΔE=3.5 meV
Intensity (counts per 72 minutes)
ξ
C
D
χ''
Energy (meV)
ξ
E
T = 35 K
T = 80 K
T = 297 K
χ''P (μB2/eV)
ΔE (meV)

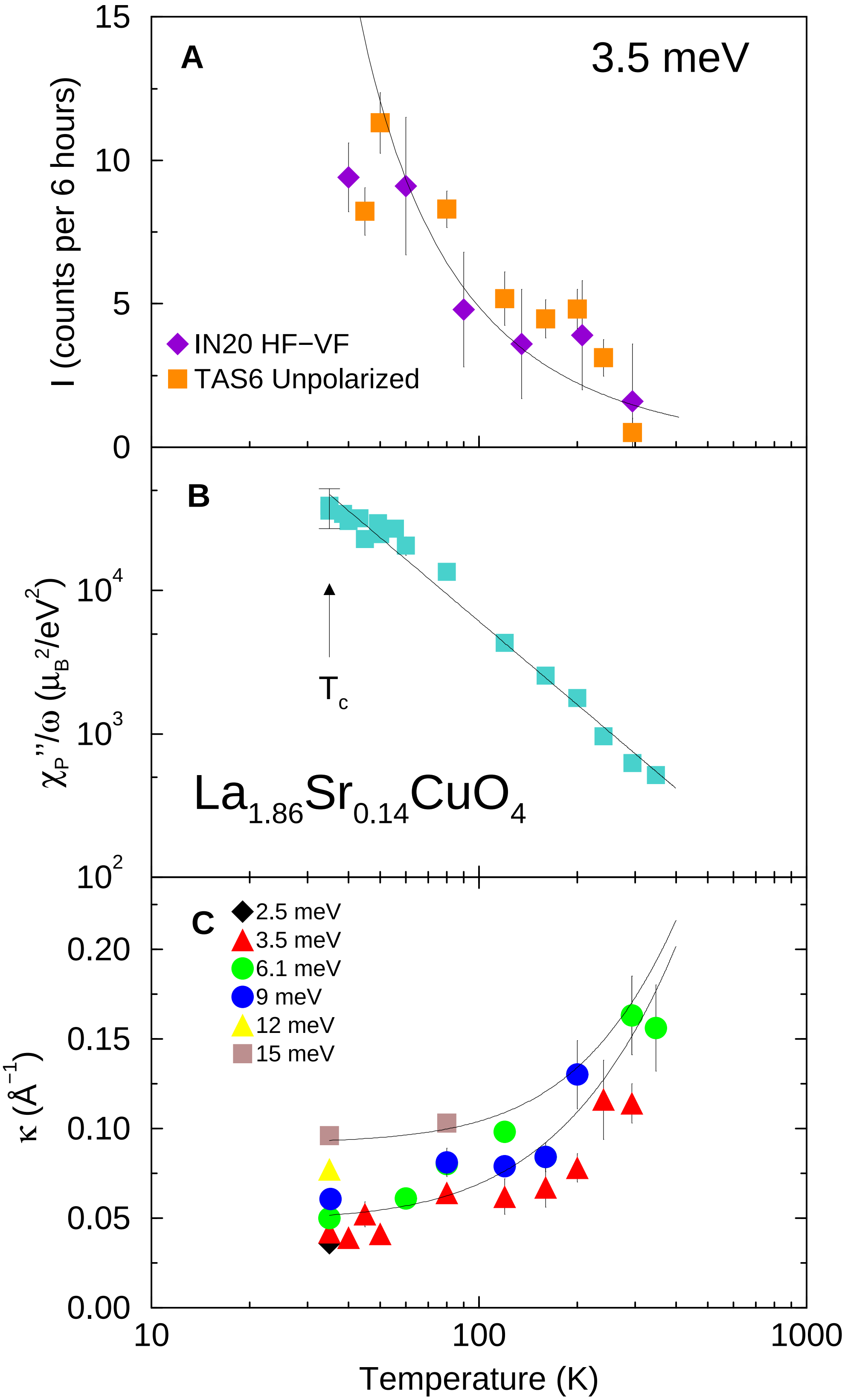

A
3.5 meV
IN20 HF−VF
TAS6 Unpolarized
I (counts per 6 hours)
15
10
5
0
B
χ_P''/ω (μ_B^2/eV^2)
10^4
10^3
10^2
T_c
$La_{1.86}Sr_{0.14}CuO_4$
C
2.5 meV
3.5 meV
6.1 meV
9 meV
12 meV
15 meV
κ ($\AA^{-1}$)
0.20
0.15
0.10
0.05
0.00
10
100
1000
Temperature (K)

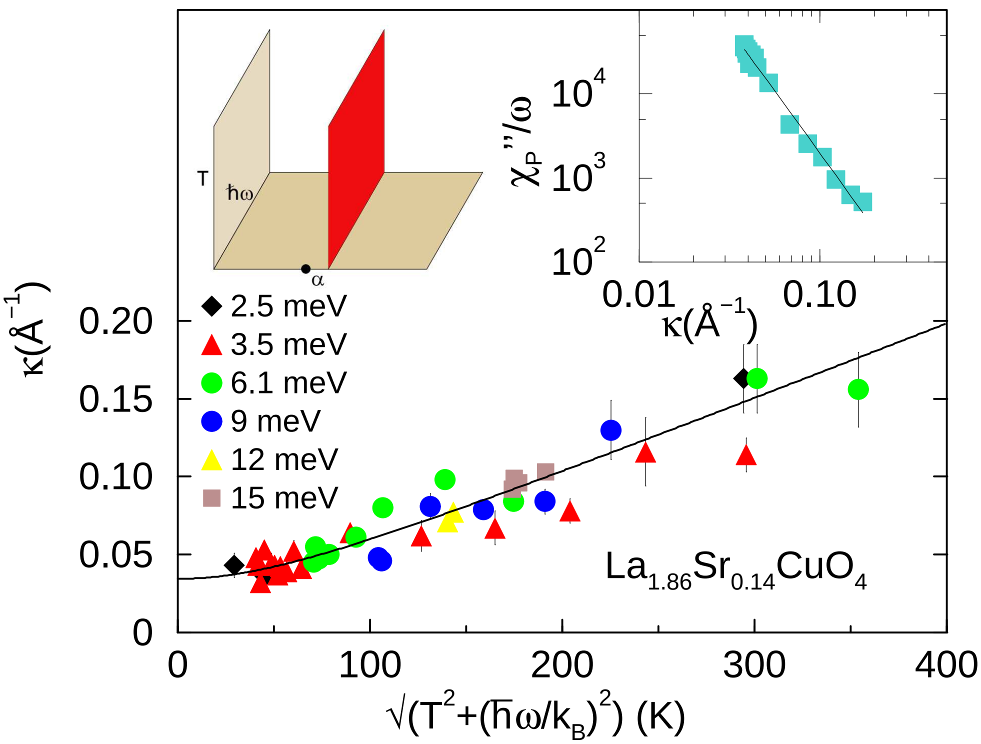

T
ħω
α
χ_P''/ω
10^4
10^3
10^2
0.01
0.10
$\kappa(\text{Å}^{-1})$
2.5 meV
3.5 meV
6.1 meV
9 meV
12 meV
15 meV
$\kappa(\text{Å}^{-1})$
0.20
0.15
0.10
0.05
0
$La_{1.86}Sr_{0.14}CuO_4$
0
100
200
300
400
$\sqrt{(T^2+(\hbar\omega/k_B)^2)}$ (K)